Chapter 5

Preparing Atoms for Interferometry

5.1 Chapter Overview

This chapter presents the stages of the experiment which prepare an ensemble of atoms for interferometry, after they are loaded into the 3D Magneto-optical Trap (MOT). After being released from the trap, the atoms are cooled and launched using a moving molasses, as described in Section 5.2. Following this, a sequence of optical and microwaves pulses is used to increase the population in the $|1,0\rangle$ ground state and end with an ensemble which has a narrow velocity spread along the Raman axis. A characterisation of this is given in Section 5.3.

Some sections of this chapter refer to parts of the experiment which have yet to be introduced. Details on the Raman laser and the velocity-selective Raman pulse can be found in Section 7.2 and Section 7.4.3, respectively. A description of the detection scheme, used to measure the population of atoms in $|F = 1\rangle$ and $|F = 2\rangle$ is presented in Section 7.3.

5.2 Cooling in Optical Molasses

A low thermal velocity means that the atoms can be interrogated for a longer time, $2T$, because the atom cloud spreads out more slowly. This in turn makes the accelerometer more sensitive because the interferometer phase is proportional to T^2. Further cooling is therefore required before the most sensitive interferometer signal can be achieved. Temperatures well below that of the Doppler limit (146 µK for Rubidium-87 (^{87}Rb)) can be reached using polarisation gradient cooling [47]. In what follows, the principles of sub-Doppler cooling using polarisation gradients will not be discussed in detail. Further details can be found elsewhere [48, 49].

This section describes the work towards to cooling and launching the atoms in a moving optical molasses. It starts with a motivation for launching the atoms in Section 5.2.1. The following section discusses the control of the intensity and frequency of the light during the molasses stage of the experiment. A description of the techniques needed to cool the atoms in a moving molasses is then given in Section 5.2.3. Finally, this section concludes in Section 5.2.4 with measurements of both the temperature and trajectory of the atom cloud which were measured using a ballistic expansion method.

5.2.1 Motivation for Launching

As previously discussed in Section 2.4.3, there are two pairs of counter-propagating beams which can drive Raman transitions between the two hyperfine ground states. If an atom can be stimulated by both pairs, then the additional trajectories this introduces do not interfere, resulting in a reduction in the fringe visibility. This problem can be avoided by using the fact that the Raman transition is Doppler-sensitive to ensure that the atoms are only driven by one pair of beams. Each pair has an opposite Doppler shift $\pm\omega_D = \pm\mathbf{k}_{\text{eff}}.\mathbf{v}$ and so their transition frequencies are separated by $2\omega_D$. Therefore,

the atoms are launched so that their centre-of-mass velocity along the Raman axis is large enough to lift the degeneracy of the two Raman transitions.

5.2.2 Frequency and Power Control

A timing diagram illustrating the power and frequency during the molasses phase is shown in Figure 5.1. After the atoms are loaded into the MOT, they are released by switching off the quadrupole field. Once this field has decayed away, the frequency and intensity of the cooling light are ramped adiabatically [50]. The frequency of the cooling light is ramped to -25Γ over 1.4 ms. Since the repump light is a sideband of the cooling light, the modulation frequency is simultaneously ramped up to keep this sideband resonant with the $|F = 1\rangle \rightarrow |F' = 2\rangle$ transition. Additionally, the relative detuning of counter-propagating MOT beams is varied so that the atoms are cooled into a moving molasses (see Section 5.2.3). After this, the intensity of the light is reduced over 5 ms. The response of the output Acousto-optic Modulator (AOM) on the μQuans laser was calibrated so that we could apply a voltage ramp that gives an approximately linear intensity ramp.

5.2.3 Launching in a Moving Molasses

The configuration for launching atoms along the Raman axis is shown in Figure 5.2. The forward-propagating beams are blue-detuned by $+\delta f_l$ and the backward-propagating ones are red-detuned by $-\delta f_l$, so that atoms with a velocity along the beam axis of $\vec{v} = \delta f_l \lambda$ are resonant with both beams. The frequency of each beam is ramped from the initial value by varying the modulation frequency of its AOM. This ramp occurs slowly to ensure strong cooling throughout the period of accelerating the atoms to their final velocity. As there is no pair of MOT beams along the axis of the Raman

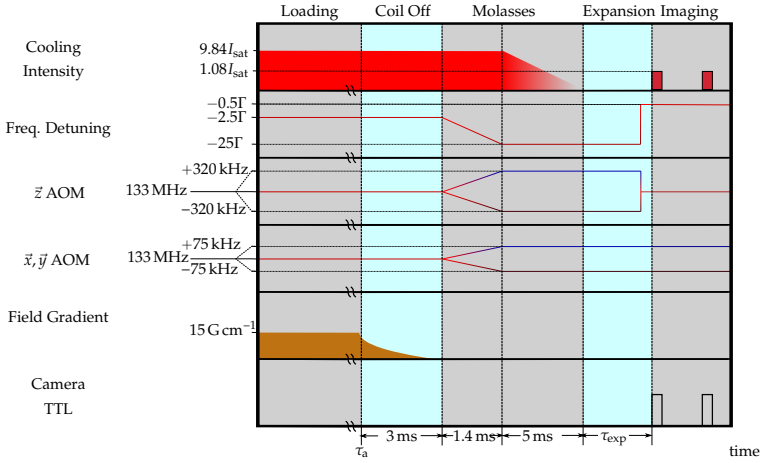

Figure 5.1: Timing diagram for the molasses stage of the experiment. After a time $\tau_a = 100$ ms, the atoms are released from the MOT. The molasses sequence begins 3 ms later, once the magnetic field from the MOT coils has decayed away. First, the frequency of the cooling light is ramped to -25Γ over 1.4 ms. The relative frequencies of counter-propagating MOT beams are detuned so that the atoms are cooled in a moving frame, launching them along a parabolic path (see Section 5.2.3). Next, the intensity of the MOT light is reduced linearly over 5 ms. To measure the temperature, the atoms are left to expand for a duration of τ_{exp} ms, after which they are imaged using the camera.

beams, the $\vec{x}$ and $\vec{y}$ MOT beams, whose axes are nominally at $\pm 45^\circ$ to the Raman axis, are used to launch the atoms. By controlling the power and alignment of each beam, the net velocity on the atoms will be along the Raman axis. If the detuning of both pairs of beams is the same, then the velocity along the Raman axis is given by $\vec{v_r} = \sqrt{2}\delta f_l \lambda$ [51].

As well as launching the atoms horizontally, the atoms are launched vertically so that they can remain closer to the centre of the chamber after the free fall time $2T$. This keeps them in a region of more uniform Raman beam intensity where the pulse area is more homogeneous across the cloud, giving better fringe visibility. This launch is carried out using the MOT beams that lie along the vertical $\vec{z}$ axis.

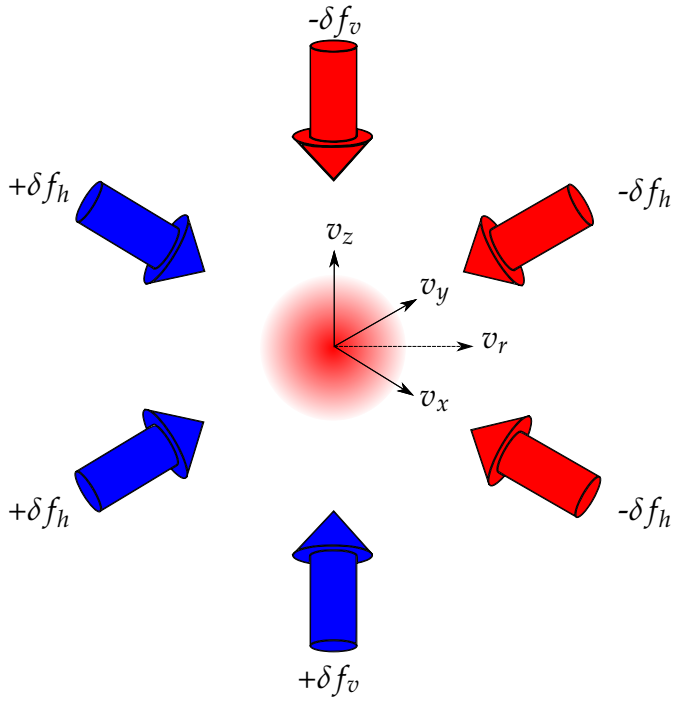

Figure 5.2: Beam configuration for a moving molasses. When counter-propagating beams are detuned from each other, the atoms are cooled into a moving frame where the Doppler shift brings both beams to the same frequency. Along the vertical axis, the beams are detuned by δf_v so that the cloud is launched upwards with a velocity $v_z = \delta f_v \lambda$. In the horizontal plane, the $\vec{x}$ and $\vec{y}$ beams are detuned by δf_h so that the resultant velocity is along the Raman axis $v_r = \sqrt{2}\delta f_h \lambda$.

5.2.4 Imaging the Atom Cloud over Time

Once released from the trap, the atom cloud is free to expand at a rate due to its thermal velocity distribution. In addition to this, the centre-of-mass moves due to its initial velocity and acceleration due to gravity (and any other external forces). The temperature of the cloud T was measured by imaging the distribution of atoms after allowing the cloud to expand in the dark for a range of expansion times. A typical atom cloud trajectory is shown in Figure 5.3, in which the cloud was imaged up to 76 ms after being released from the trap.

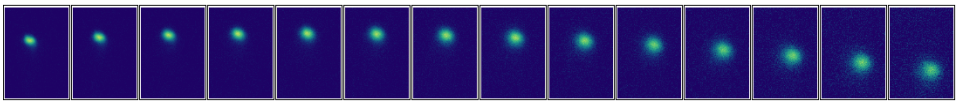

Figure 5.3: A series of images showing the trajectory of the atom cloud after being cooled in a moving molasses. The first image was taken 7 ms after initiating the molasses and a subsequent one every 5 ms. Each image represents a region of interest of dimensions 1150 × 1650 pixels that covers the spatial extent of the atom cloud during the launch.

Measuring the Temperature

In thermal equilibrium, the velocity distribution of the atoms is described by a Maxwell-Boltzmann distribution. The velocity component along one direction has the distribution

$$f(v_x) = \left(\frac{m}{2\pi k_B T}\right)^{1/2} e^{-\frac{m(v_x - \langle v_x \rangle)^2}{2k_B T}} \tag{5.1}$$

Assuming that the number density is initially a Gaussian, with a peak number density $n_0(x_0)$ at the centre-of-mass, and a mean square radius projected along x of σ_0^2, the number density (projected along x) at later times is given by a convolution with equa-

tion (5.1)

$$n(x,t) = \int n_0(x_0) \left(\frac{m}{2\pi k_B}\right)^{1/2} e^{-\frac{m(v_x-\langle v_x\rangle)^2}{2k_BT}} e^{-\frac{(x+v_xt-x_0)^2}{2\sigma_0^2}} \mathrm{d}v_x \tag{5.2}$$

where σ_0 is the $1/e^2$ initial width of the cloud. As a convolution of two Gaussians, equation (5.2) is also a Gaussian, with a $1/e^2$ width given by

$$\sigma(t)^2 = \sigma_0^2 + \frac{k_BT}{m}t^2 \tag{5.3}$$

Figure 5.4 shows a typical density profile projected along each axis seen by the camera, as described in Section 4.2.3. The width along each axis is estimated using a non-linear least squares fit to equation (5.2). Figure 5.5 shows the measured cloud width over a range of expansion times. The initial measurement was made 7 ms after the end of the molasses to allow for enough time to re-lock the laser to -0.5Γ below the $|F=2\rangle \rightarrow |F'=3\rangle$ transition and align the bias field to the $\vec{z}$ axis so that the atoms could be optically pumped into the $|2,2\rangle$ state. The slopes of these graphs give the temperatures along the horizontal and vertical axes of the camera as $T_x = 6.38(11)\,\mu\mathrm{K}$ and $T_y = 6.38(9)\,\mu\mathrm{K}$, respectively.

Measuring the Launch Trajectory

The same method used to measure the temperature of the cloud can also be used to measure the position of the centre-of-mass. In this case, the quantity of interest is $\langle x(t)\rangle$. Since the cloud is in free-fall, the trajectory for the centre-of-mass is then given by the well-known equation-of-motion for a particle moving under constant

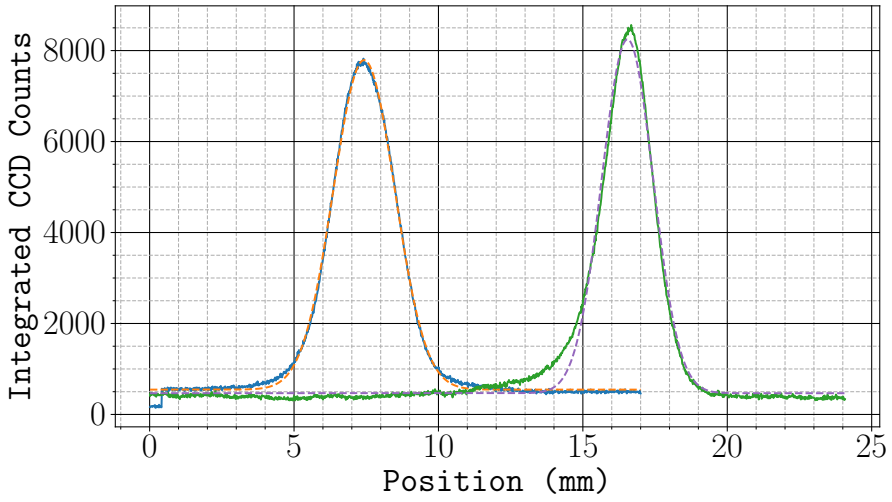

Figure 5.4: Integrated pixel count for a single image during ballistic expansion. The dashed lines indicate non-linear least squares fits to a Gaussian function.

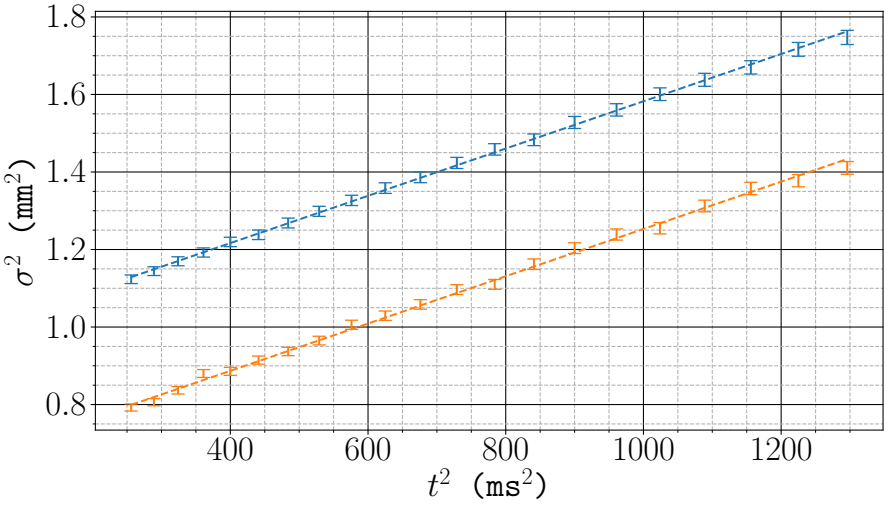

Figure 5.5: Mean squared cloud radius plotted against the square of the ballistic expansion time. After molasses, the cloud is left to expand in the dark and in a region of close to zero magnetic field. Least-squares fits to the camera images give the mean-square radii $\sigma(t)^2$ in the horizontal (blue) and vertical (orange) directions. The gradient of these curves gives temperatures $T_x = 6.38(11)\,\mu\text{K}$ and $T_y = 6.38(9)\,\mu\text{K}$.

acceleration

$$\langle x(t)\rangle = \langle x(0)\rangle + v_x t + \frac{1}{2}a_x t^2 \tag{5.4}$$

where v_i is the initial velocity along the given axis and a_i is the acceleration.

To launch the atoms vertically, the (z_+, z_-) AOMs were ramped so that the frequency difference between the light beams was 2×320 kHz. To launch along the Raman beams, the x and y AOM frequencies were ramped to give a frequency difference of 2×75 kHz between each pair of horizontal MOT beams. Figure 5.6 is a plot of the measured centre-of-mass position along the horizontal and vertical camera axes over time. A linear least-squares fit to equation (5.4) gives a vertical launch quantities of $v_v = 25.00(24)\,\mathrm{cm\,s^{-1}}$ and $a_v = -9.400(51)\,\mathrm{m\,s^{-2}}$ and $v_h = 7.39(14)\,\mathrm{cm\,s^{-1}}$ and $a_h = -0.320(36)\,\mathrm{m\,s^{-2}}$ along the horizontal axis.

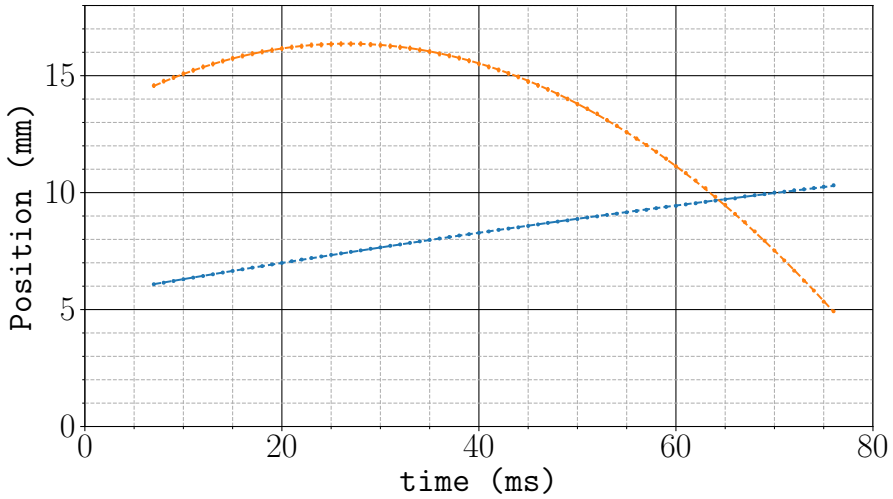

Figure 5.6: Measured centre-of-mass position over time. The horizontal component of the position is shown in blue and the vertical in orange. Each trajectory is fit to equation (5.4) to estimate the launch velocity. The best-fit values are $v_v = 25.00(24)\,\mathrm{cm\,s^{-1}}$ and $a_v = -9.400(51)\,\mathrm{m\,s^{-2}}$ along the vertical axis and $v_h = 7.39(14)\,\mathrm{cm\,s^{-1}}$ and $a_h = -0.310(36)\,\mathrm{m\,s^{-2}}$ along the horizontal.

When compared to the expected velocities from the detunings, $v_v^{(l)} = 24.96\,\mathrm{cm\,s^{-1}}$ and $v_h^{(l)} = 5.85\,\mathrm{cm\,s^{-1}}$, the measured horizontal velocity is far greater than expected. This can be explained by a residual magnetic field, that is not cancelled using the bias coils. In the presence of a magnetic field, atoms cooled in an optical molasses are decelerated to a velocity at which the Zeeman shift is cancelled by the Doppler shift. This velocity-selective resonance depends on the orientation of the magnetic field to the polarisation of the light. In a one-dimensional optical molasses, a resonance occurs at $v_{\mathrm{res}}^{(1)} = -\mu_B g_F B/\hbar k$ when the magnetic field is aligned with the wavevector of the light [52]. When the field is aligned at an arbitrary angle an additional resonance at $v_{\mathrm{res}}^{(2)} = -\mu_B g_F B/2\hbar k$ is present, due to additional $\left(\sigma^{\pm} - \pi\right)$ transitions [53, 54]. A residual field along the Raman axis of 20 mG would shift the resonance along $\vec{x}$ and $\vec{y}$ by $1.09\,\mathrm{cm\,s^{-1}}$ corresponding to a velocity of $1.54\,\mathrm{cm\,s^{-1}}$ along the Raman axis. The magnetic field inside the chamber is controlled using bias coils and no attempt was made to cancel magnetic field gradients. It is plausible that a residual field of this magnitude is a result of a magnetic field gradient. For the moment, this does not cause a problem as we simply adjust the molasses detuning to achieve the desired launch velocity. In future, a precisely known launch velocity may be required for sensing rotations, and then it will be necessary to return to this issue.

5.3 State Preparation

After the atoms have been cooled in an optical molasses, the population will mostly be distributed across the $|F = 2\rangle$ level, along with a small fraction distributed across the $|F = 1\rangle$ level. The Raman transition only couples the $|1, 0\rangle$ and $|2, 0\rangle$ states, so atoms in the other hyperfine ground states cannot participate in the interferometer. In fact, since the individual Zeeman sub-levels are not resolved during detection, these background atoms result in a loss of fringe visibility. One way to overcome this is to apply a pulse

of light resonant with the $|F = 2\rangle \rightarrow |F' = 3\rangle$ transition to push the non-participating atoms out of the interferometer detection region. Of course, this must be done after applying a Raman pulse to transfer an ensemble of atoms from $|2, 0\rangle$ into $|1, 0\rangle$. In this simple scheme a large fraction of the atoms are removed, which is undesirable since measurements of a low number of atoms are inherently more uncertain due to shot number fluctuations.

The following section discusses a method of preparing the atoms to increase the population in the $|1, 0\rangle$ ground state. An overview of the scheme is given in Section 5.3.1. This is followed by a discussion of the initial steps which optically pump atoms into the $|1, 0\rangle$ state in Section 5.3.2. A description of the microwave pulse used to drive atoms into the $|F = 2\rangle$ level is given in Section 5.3.3. This section concludes with the method used to blow away the atoms which do not contribute to the interferometer in Section 5.3.4. A key step which has been omitted is the velocity-selective Raman pulse. This is described in more detail later, in Section 7.4.3.

5.3.1 Schemes for Preparation

The scheme used to prepare atoms in the $|1, 0\rangle$ state is the following:

1. Light resonant with the $|F = 2\rangle \rightarrow |F' = 2\rangle$ transition pumps atoms into the $|F = 1\rangle$ level
2. Light resonant with the $|F = 1\rangle \rightarrow |F' = 0\rangle$ transition drives ($\sigma^{\pm}$) transitions to pump atoms into the $|1, 0\rangle$ dark state
3. A microwave π-pulse transfers atoms to $|2, 0\rangle$
4. A Raman π-pulse transfers atoms with a narrow velocity spread back to $|1, 0\rangle$
5. The atoms which remain in $|F = 2\rangle$ are blown away

A diagram of the population of each hyperfine ground state and the laser frequencies used to drive these transitions is given in Figure 5.7. With the exception of step 4, the light is provided by the μQuans laser using the MOT collimators aligned to the vertical $\vec{z}$ axis. The frequency of the cooling laser and the repump sideband are set so that the relevant transitions for steps 1 and 2 are addressed. As the $|F = 1\rangle$ light is a sideband of the $|F = 2\rangle$ light, it is not possible to blow away atoms in $|F = 1\rangle$ without also blowing away atoms in $|F = 2\rangle$. This problem is overcome by using microwave pulses to drive atoms up to $|F = 2\rangle$ before velocity selection.

A timing diagram of the state preparation sequence is shown in Figure 5.8, which indicates the duration for which each optical or microwave pulse is applied, as well as the direction of the applied magnetic field. The field is switched slowly over 2 ms (which is omitted from the diagram) to preserve the spin state of each atom.

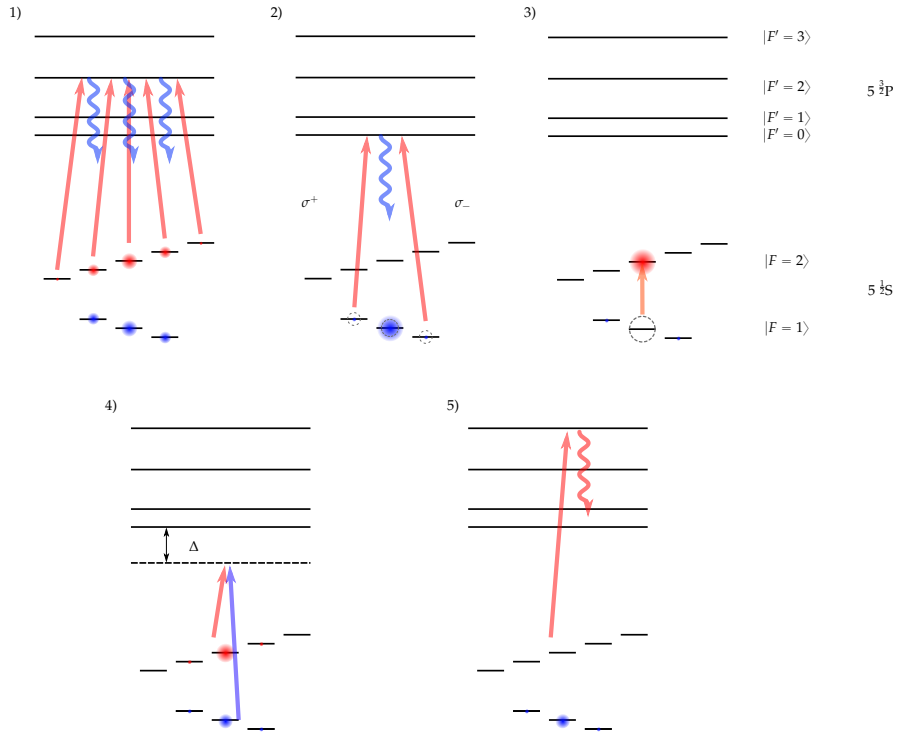

Figure 5.7: Sequence of optical and microwave pulses used to prepare an ensemble of atoms in $|1, 0\rangle$. The red arrows indicate optical transitions to and from $|F = 2\rangle$ and equivalently for the blue arrows and $|F = 1\rangle$. A residual population in the $|1, \pm 1\rangle$ states is present, which contributes to a background during the interferometer.

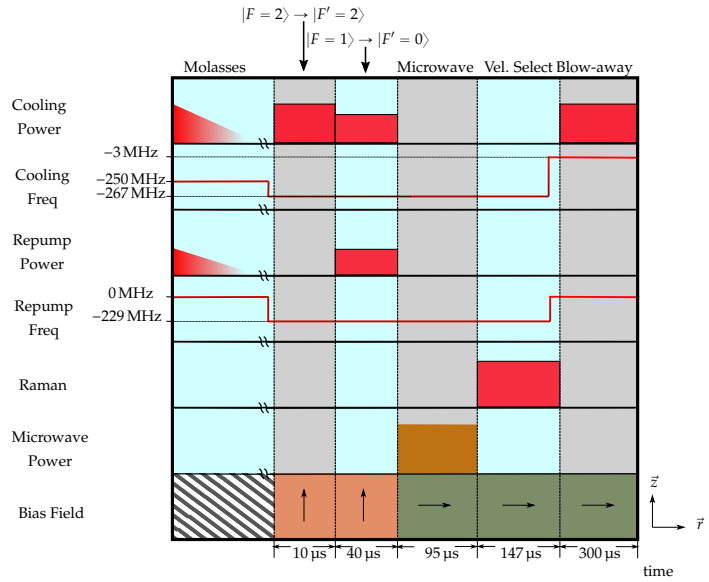

Figure 5.8: Timing diagram for state selection sequence. The durations labelled are indicative of the time required to drive the atoms into the desired state at each step. After the $|F=1\rangle \rightarrow |F'=0\rangle$ pumping, the magnetic field is re-oriented along the Raman axis $\vec{r}$. The 2 ms field switching time has been omitted.

5.3.2 Optically Pumping the Atoms

Driving the $|F=2\rangle \rightarrow |F'=2\rangle$ transition

After the molasses, the frequency of cooling light is 150 MHz below the $|F=2\rangle \rightarrow |F'=3\rangle$ transition. This can off-resonantly excite an atom to the $|F'=2\rangle$ excited level, but the small scattering rate means that on average, an atom will need to scatter many photons before it is pumped into the $|F=1\rangle$ level. Therefore, to minimise the heating during this pumping process, the frequency of the cooling light is resonant with the $|F=2\rangle \rightarrow |F'=2\rangle$ transition.

Figure 5.9 shows the population in the two hyperfine ground states as the duration of the $|F=2\rangle \rightarrow |F'=2\rangle$ light is increased. The rate at which atoms are pumped into $|F=1\rangle$ increases with the strength of the applied magnetic field. At zero field, there exists a dark state which is a coherent superposition of the $|2,m_F\rangle$ states [55]. Applying a magnetic field lifts the degeneracy between the Zeeman sub-levels so that this dark

state is no longer stationary. The evolution rate of this dark state, and hence pumping rate, increases with an increasing Zeeman shift. At a field strength of 3 G, the atoms can be pumped into $|F = 1\rangle$ in less than 5 µs.

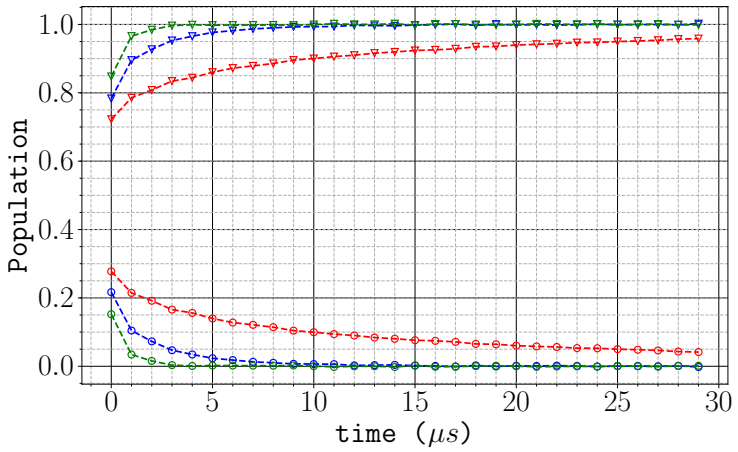

Figure 5.9: Population across the two hyperfine ground states after $|F = 2\rangle \rightarrow |F' = 2\rangle$ pumping under various magnetic field strengths. The ▿ (○) markers indicate the population in $|F = 2\rangle$ ($|F = 1\rangle$). The red, blue and green series correspond to field strengths of −0.16 G, 1.67 G, and 3 G, respectively.

Driving the $|F = 1\rangle \rightarrow |F' = 0\rangle$ transition

After this first pumping step, the atoms are distributed across the Zeeman sub-levels in $|F = 1\rangle$. The next pulse of light is used to increase the population in $|1, 0\rangle$ by driving $|F = 1\rangle \rightarrow |F' = 0\rangle$ transitions. During this time, the $|F = 2\rangle \rightarrow |F' = 2\rangle$ light remains on which helps to prevent atoms from populating the $|F = 2\rangle$ level through off-resonant $|F = 1\rangle \rightarrow |F' = 1\rangle$ excitations. The magnetic field present means that the circularly-polarised $\vec{z}$ MOT beams only drive $\sigma^{\pm}$ transitions, so the $|1, 0\rangle$ state is in principle a dark state.

The distribution of atoms across the Zeeman sublevels was measured using a microwave pulse to drive atoms into the $|F = 2\rangle$ level, which is described in Section 5.3.3.

For each π microwave transition, the frequency of the microwave field was varied to find the resonant frequency. The resulting spectra for $m_F = -1$ and $m_F = 0$ are shown in Figure 5.10, both with and without applying light to pump into the $|1,0\rangle$ state. The $0 \rightarrow 0$ clock transition is detuned from the hyperfine splitting frequency due to the applied magnetic field, giving a second-order Zeeman shift of $515\,\mathrm{Hz\,G^{-2}}$. The measured shift of 5.6 kHz corresponds to a field strength of 3.3 G.

A plot of the population in each Zeeman sub-level for increasing pumping times is given in Figure 5.11. In this instance, the optical pumping does not completely deplete the population from the $m_F = \pm 1$ sub-levels. After pumping for 30 µs, approximately 5% of the population remains in the $m_F = \pm 1$ sub-levels. The $|1,0\rangle$ state can only be excited to $|F' = 0\rangle$ by π-polarised light, which suggests that the magnetic field is mis-aligned with the $\vec{z}$ MOT beams. The effect of these background atoms on the measured interferometer signal is discussed later, in Section 7.3.3.

5.3.3 Including Microwave Transitions

Without a dedicated laser to drive transitions from the $|F = 1\rangle$ level, it was necessary to implement a scheme to use light resonant with the $|F = 2\rangle$ level to remove background atoms. Therefore, we included a system for driving microwave frequency transitions from $|1,0\rangle$ to $|2,0\rangle$.

Microwave Generation

A diagram of the setup for this is shown in Figure 5.12. The microwave radiation is generated using a *Wind-Freak* synthesiser to output a microwave field oscillating at a frequency close to the hyperfine splitting frequency, $f_{\mathrm{hfs}} = 6.838\,46\,\mathrm{GHz}$. This is amplified by *MiniCircuits MCL ZRON-8G+* amplifier and directed into the chamber

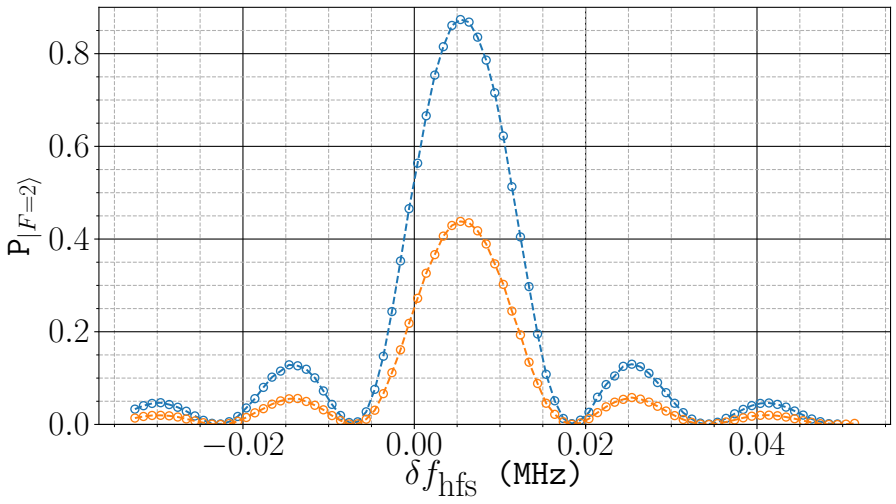

(a)

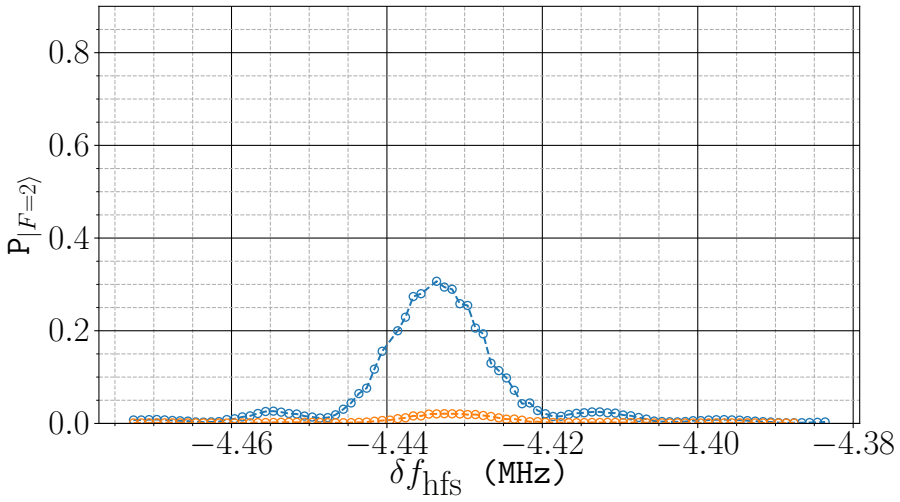

(b)

Figure 5.10: Population of atoms in (a) $|1,0\rangle$ and (b) $|1,-1\rangle$, measured by applying a 68 µs microwave pulse to drive atoms into the $|F=2\rangle$ level. The orange and blue points indicate the measured populations with and without $|F=1\rangle \rightarrow |F'=0\rangle$ pumping. The microwave frequency is plotted as a detuning from the hyperfine splitting frequency f_{hfs}.

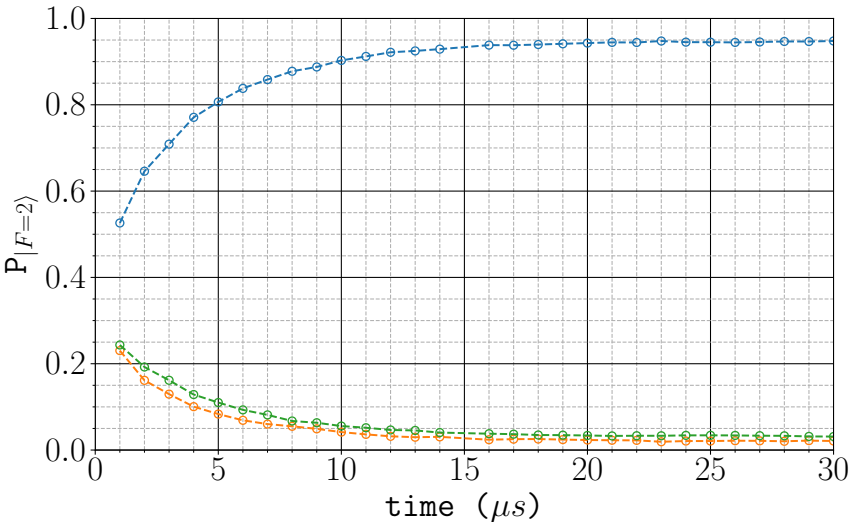

Figure 5.11: Population in each Zeeman sub-level as the $|F = 1\rangle \rightarrow |F' = 0\rangle$ pumping time is increased. The $m_F = 0, -1, +1$ populations are shown in blue, orange and green, respectively. After 30 µs, approximately 5% of the population remains in the $m_F = \pm 1$ sub-levels.

using a *Pasternack PE9859/SF-10* microwave horn, which produces a linearly-polarised microwave field. The horn was aligned to the chamber at the position which maximised the population of atoms in the $|2, 0\rangle$ state. The synthesiser is clocked using a stable 100 MHz signal from the μQuans laser. When the synthesiser was clocked using its internal 27 MHz reference clock, this produced a noticeable jitter in the output frequency, which led to a significant shot-to-shot fluctuation in the $|2, 0\rangle$ population.

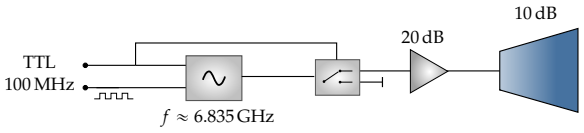

Figure 5.12: Schematic diagram of the microwave assembly. The frequency close to the hyperfine splitting frequency is generated by a *Wind-Freak* synthesiser. A 100 MHz clock signal acts as a stable reference frequency for the synthesiser. The generated microwave power is amplified twice, first by a low-power *Mini-Circuits* amplifier, then by a microwave horn, which produces a highly directional, linearly polarised wave. The output is controlled by a digital signal, both at the synthesiser and at a bi-directional microwave switch. The second port of this is blocked with a 50 Ω terminator to prevent reflections.

Pulse Characterisation

Figure 5.13 shows a measurement of the population in the $|F = 2\rangle$ level for increasing durations duration of the applied microwave pulse. Rabi oscillations between the $|1, 0\rangle$ and $|2, 0\rangle$ states are clearly present. The loss of coherence between the states can be explained by an inhomogeneous driving field. Once inside the chamber, the microwaves reflect and scatter off the interior surfaces which results in a spatially-dependent Rabi frequency. This also leads to a depolarisation of the field, as $\sigma^{\pm}$ transitions were also observed. Initially, around 85% of the population was driven into $|F = 2\rangle$ using a microwave pulse of 100 µs. After improving the alignment of the magnetic field during the microwave pulse, this fraction increased to 97% - the remaining 3% being distributed across the $m_F = \pm 1$ states.

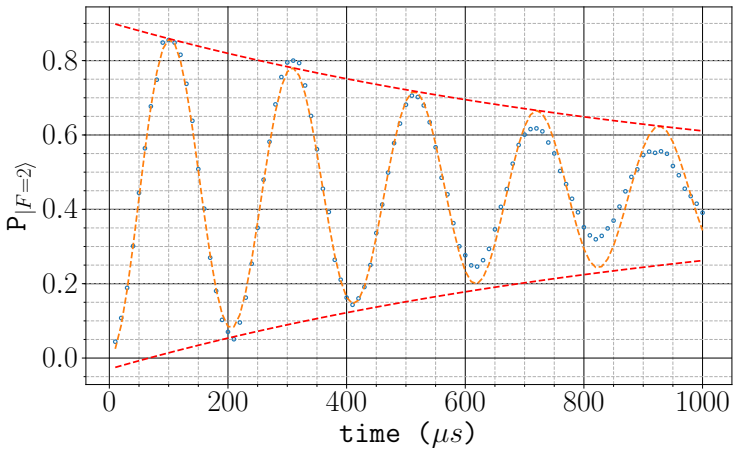

Figure 5.13: Damped Rabi oscillation between $|1, 0\rangle$ and $|2, 0\rangle$ using a microwave pulse of varying length. At longer pulse times, there is a loss of coherence due to a dephasing between the two states. The red dashed line is an envelope is a fit to a decaying exponential with a characteristic time of $\tau = 1016$ µs.

Figure 5.14a shows a spectrum obtained by varying the frequency of the microwave pulse. This shows the presence of $\Delta m = \pm 1$ transitions from $|1, 0\rangle$, as well as the fact that the population in $|1, m_F = \pm 1\rangle$ decreases after the $|F = 1\rangle \rightarrow |F' = 0\rangle$ pumping step is applied. The linewidth of the microwave transition is much narrower than the

Zeeman splitting, so only the clock transition is driven when a pulse with a frequency close to f_{hfs} is applied.

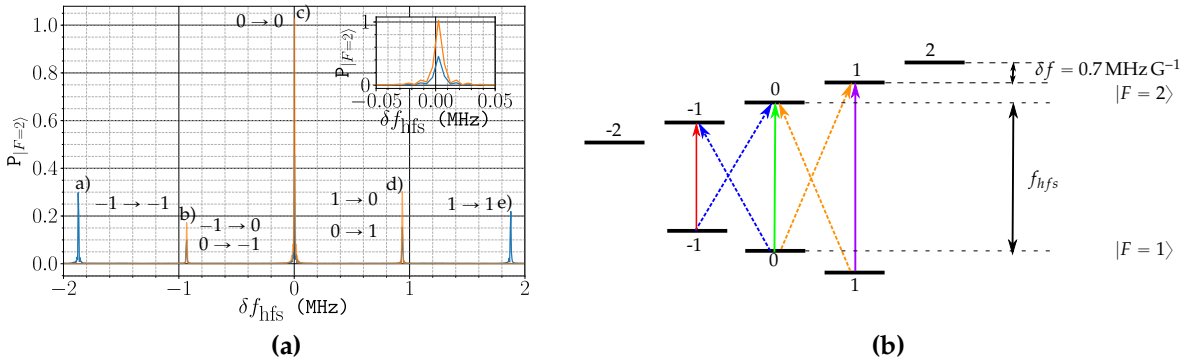

Figure 5.14: (a) shows the microwave transition spectrum before (blue) and after (orange) $|F = 1\rangle \rightarrow |F' = 0\rangle$ pumping. **(b)** shows the transitions addressed as the microwave frequency is varied. Dashed and lines indicate $\Delta m = \pm 1$ transitions and solid lines indicate $\Delta m = 0$. In order of increasing frequency, the transitions in **(a)** are highlighted in: a) red, b) blue, c) green, d) orange and e) purple.

5.3.4 Blow-Away

After the atoms populate $|2, 0\rangle$, a velocity-selective Raman π-pulse is applied to transfer a fraction of those back into $|1, 0\rangle$ [56]. This step is discussed in detail in Section 7.4.3. The velocity-selective Raman pulse transfers 4% the atoms back to $|1, 0\rangle$. The remaining need to be removed, otherwise they contribute to a large background signal.

The final pulse during the state preparation sequence is used to push these non-contributing atoms out of the interferometer region. A single MOT beam is used so that there is a net momentum transfer to the atoms as they absorb light and fluoresce. The frequency of this blow-away beam is detuned from the $|F = 2\rangle \rightarrow |F' = 3\rangle$ transition by −3 MHz, which is the same frequency used for detection (see Section 7.3). A pulse of 50 µs is enough to remove all atoms in $|F = 2\rangle$.

5.4 Conclusion

This chapter has presented the stages of the experiment which are used to prepare an ensemble of atoms for interferometry. This requires cooling the atoms to limit the thermal expansion of the cloud during interferometry. The atoms are also launched using a moving molasses so that only one pair of beams is resonant with the Raman transition. Finally, we then apply a sequence of optical and microwave pulses, to increase the population of atoms in $|1,0\rangle$. A velocity-selective Raman pulse with a narrow linewidth is used to make the velocity spread along the Raman axis much smaller than the Doppler width. Aside from some residual population in $|1,\pm1\rangle$, the remaining atoms are removed using a pulse of light close to resonance with the $|F=2\rangle \rightarrow |F'=3\rangle$ transition. This results in an ensemble of which around 40% of the population contributes to the interferometer signal.